引用格式：ZHU Yan-xu，YANG Zhuang，SONG Hui-hui，*et al*. Preparation and Optimization of Photosensitive Gate GaN-based High Electron Mobility Transistor Devices[J]. *Acta Photonica Sinica*，2020，**49**(6)：0604002
朱彦旭，杨壮，宋会会，等.基于感光栅极 GaN 高迁移率晶体管的新型探测器制备与优化[J].光子学报，2020，**49**(6)：0604002

基于感光栅极 GaN 高迁移率晶体管的新型探测器制备与优化

朱彦旭，杨壮，宋会会，李赉龙，杨忠，李琦轩，胡铁凡
（北京工业大学 光电子技术教育部重点实验室，北京 100124）

摘　要：利用 GaN 高电子迁移率晶体管（HEMT）的栅控特性和锆钛酸铅（PZT）铁电薄膜的光伏效应，在 HEMT 器件的栅极处沉积一层 PZT 铁电薄膜，提出了一种新型的（光敏感层/HEMT）探测结构.为制备出光伏性能优异的薄膜，对不同的溅射功率和退火温度制备的 PZT 铁电薄膜进行表面形貌和铁电性能分析.发现 200 W 溅射功率、700 ℃的退火温度制备的薄膜表面晶粒生长明显，剩余极化强度为 38.0 μC·cm^{-2}.工艺制备 GaN 基 HEMT 器件并把 PZT 薄膜沉积到器件栅极上.在无光和 365 nm 紫外光照射下对有、无铁电薄膜的 HEMT 探测器的输出特性进行测试.结果显示，在光照时，有铁电薄膜的 HEMT 器件相较于无光时，源-漏饱和电压最多降低 3.55 V，饱和电流最多增加 5.84 mA，表明新型感光栅极 HEMT 探测器对紫外光具有优异的探测效果.为实现对新型探测器的结构进行优化的目的，对栅长为 1 μm、2 μm 和 3 μm 等不同栅长的探测器进行光照测试.结果表明，在紫外光照射下，三种探测器的漏极饱和电流分别为 23 mA、20 mA 和 17 mA，所以栅长越长器件的饱和电流越小，探测性能越差.

关键词：量子光学；光学探测器；光伏效应；铁电薄膜；氮化镓；紫外线源；光刻
中图分类号：O472.3　　**文献标识码**：A　　**doi**：10.3788/gzxb20204906.0604002

Preparation and Optimization of Photosensitive Gate GaN-based High Electron Mobility Transistor Devices

ZHU Yan-xu，YANG Zhuang，SONG Hui-hui，LI Lai-long，YANG Zhong，LI Qi-xuan，HU Tie-fan
(*Key Laboratory of Photoelectron Technology Ministry of Education*，*Beijing University of Technology*，*Beijing* 100124，*China*)

Abstract：Based on the gate controlled characteristics of GaN High Electron Mobility Transistors (HEMTs) and on the photovoltaic effect in lead zirconate-titanate(PZT) ferroelectric thin films，a new type of photosensitive layer/HEMT detector structure is proposed. For this purpose，a PZT ferroelectric thin film is deposited on the gate of a HEMT device to prepare films with optimized photovoltaic performance，the surface morphology and ferroelectric properties of PZT films prepared by different sputtering powers and annealing temperatures are analyzed. It is found that the best conditions for the grain growth on the surface of the film are at 200 W sputtering power and 700 ℃ annealing temperature，and the residual polarization intensity is 38.0 μC·cm^{-2}. The output characteristics of the fabricated photosensitive gate PZT/GaN-based HEMT devices are compared to those of pristine HEMTs under both dark condition and 365 nm ultraviolet light. The results show that the source drain saturation voltage of

Foundation item：National High Technology Research and Development Program of China (No.2015AA033305)，National Key Reserach and Development Program of China (Nos.2017YFB0402800，2017YFB0402803)

First author(Corresponding author)：ZHU Yan-xu(1977－)，male，associate professor，Ph.D degree，mainly focuses on GaN HEMT devices and lasers.Email：zhuyx@bjut.edu.cn

Received：Dec.16，2019；**Accepted**：Apr.3，2020

the HEMT with the ferroelectric thin film decreases by 3.55 V and the saturation current increases by 5.84 mA, compared with those without light, clearly indicating a significant UV photodetection capability. To achieve the purpose of optimizing the structure of the new type of detector, detectors with different grid lengths such as 1 μm, 2 μm, and 3 μm are tested. The results show that under ultraviolet light, the drain saturation currents of the three detectors are 23 mA, 20 mA, and 17 mA, respectively. Therefore, the longer the gate length, the smaller the saturation current of the device, and the worse the detection performance.

Key words: Quantum optics; Optical detectors; Photovoltaic effects; Ferroelectric thin films; Gallium hitride; Ultraviolet sources; Lithography

OCIS Codes: 040.5160; 040.7190; 310.2790; 310.6860

0 Introduction

Photodetectors are a type of optoelectronic devices which convert optical radiation signals into another form of signals that can be easily received and processed, and are widely used in medical, military, remote sensing imaging, and many other industries[1]. Sensitivity and gain impose significant constraints to the development of photodetectors, and many researchers are trying to overcome this issue. Recently, n-Si/p^{+-B} photodiodes of a very high sensitivity and stability have been demonstrated, but they still exhibit responsivity in the order of $\sim 10^{-1}$ A/W[2]. YANG Zhen-qian [3] et al from Peking University designed a high-performance Single Crystalline - Thin Film (SC-TF) perovskite photodetector with detection power and gain bandwidth increased by two and four orders of magnitude, respectively. However, the performance of perovskite-type devices based on polycrystalline thin film active layers still lags behind epitaxially grown semiconductor devices.

GaN-basedHigh Electron Mobility Transistors (HEMTs) are epitaxial semiconductor devices, which typically consist of an AlGaN/GaN heterostructure. The AlGaN/GaN heterojunction itself exhibits a spontaneous and piezoelectric polarization. Such strong polarization creates a large amount of 2-dimensional Electron Gas (2-DEG) at the heterojunction, even if the AlGaN control layer is not doped[4], and the electron mobility can reach 2 000 $cm^2/(V \cdot s)$[5].The detectors fabricated using GaN-based HEMT devices have the advantages of high sensitivity and wide detection surface, and have increasingly become the focus of novel detector research[6].

The source to drain voltage in the GaN-based HEMT device forms an electric field which acts on the 2-DEG to form an output current. When the gate voltage changes, the concentration and the mobility of the 2-DEG change accordingly. It can be seen that once the source-drain voltage is determined, the source-drain current is dependent only on the gate voltage. Thus, the GaN-based HEMT is a typical gate control device. Researches on HEMT based devices to make detectors focus on the gate control characteristics. In 2015, researchers[7] used H_2O_2 to oxidize the GaN surface at the gate position in order to change the gate voltage, thereby implementing a detector for hydrogen detection. In 2019, LI JIN-lun et al from Chinese Academy of Sciences[8] prepared a terahertz detection device coupled with a butterfly antenna to achieve terahertz detection. To date, there are only few studies on photodetectors based on GaN-based HEMTs. In 2019, a group from Dongguk University in South Korea[9] developed a detector structure by growing ZnO nanorods on the gate of a HEMT. Oxygen adsorbed on the surface of the nanorods in the dark will generate a negative gate potential. When irradiated with ultraviolet (UV) light, the decrease in adsorbed oxygen results in a decrease in negative charge, and the purpose of detecting ultraviolet light is in turn achieved. However, practical applications of ZnO are significantly limited to ultraviolet light, due to the large bandgap (~3.2 eV), and this type of detector is only suitable for the detection of UV light, which is not conducive to broad-spectrum detection and has poor scalability. Moreover, ZnO nanorods place stringent requirements on the fabrication process.

Ferroelectric materials are novel functional materials, and Piezoelectric Ceramic Transducer (PCT) is one of them. Due to their ferroelectric, piezoelectric, thermoelectric, electro-optic, etc., properties, the ferroelectric materials can be used in a variety of device applications, like sensor devices, optoelectronic devices, and various types of memory devices[10]. Ferroelectric materials have high dielectric constant and

residual polarization[11]. Moreover, ferroelectric films exhibit a photovoltaic effect[12-13]. As a matter of fact, since the positive and negative charge centers in ferroelectrics do not coincide, even without an applied electric field electric dipole moments can be generated, that is, spontaneous polarization occurs[14-15]. When a light of a certain wavelength illuminates the ferroelectric, the electrons in the valence band are excited to transition to the conduction band, and electron-hole pairs are generated. Under the influence of the spontaneous polarization, the electrons and the holes move to the two respective poles, thereby generating photocurrent and photovoltage.

In this paper, a new method to change the gate voltage of a HEMT device under light irradiation is proposed to design a new type of photodetector structure. With the aim of combining a GaN-based HEMT with a ferroelectric PZT thin film exhibiting a photovoltaic effect, a PZT thin film is deposited on the gate of the HEMT device to form a novel PZT/GaN-based HEMT detector structure. When the light is irradiated onto the ferroelectric thin film, the latter generates an electric field due to the photovoltaic effect, thereby causing the gate to generate an additional electromotive force. A change in the gate voltage entails a change in the field strength at the AlGaN/GaN interface, that ultimately leads to a change in the 2-DEG[16]. As a result, the source-drain saturation current of the device, in turn, changes, and the purpose of detecting light is finally achieved.

The following relevant features can be pointed out: 1) Ferroelectric thin films have obvious photovoltaic effects, and the 2-DEG of the GaN-based HEMT device is extremely sensitive to changes in the gate electricfield. Expectedly, the resulting detectors exhibit a high detection rate. 2) The GaN-based HEMT devices are sensitive to input signals, thus reducing the process difficulty due to the thermal insulation of the ferroelectric thin films. 3) A simple planar device structure is required, with no need of micro-motion components, and low vibration/sound interference. 4) The structure is highly expandable, and a wide-spectrum detection can be achieved by changing the photosensitive film, which is favorable for the development of ultraviolet-visible-infrared detectors.

In this paper, based on the gate controlled characteristics of GaN high electron mobility transistors and on the photovoltaic effect in lead zirconate-titanate ferroelectric thin films, a new type of photosensitive layer/HEMT detector structure is proposed. Firstly, in order to prepare films with optimized photovoltaic performance, the surface morphology and ferroelectric properties of PZT films prepared by different sputtering powers and annealing temperatures are analyzed. Secondly, Photosensitive gate GaN HEMT device is prepared , and the output characteristics of the fabricated photosensitive gate PZT/GaN-based HEMT devices are compared to those of pristine HEMTs under both dark condition and 365 nm ultraviolet light. The results show that the new photosensitive gate GaN HEMT detector responds significantly to ultraviolet light. Finally, several HEMT detectors with photosensitive gates of different lengths are also prepared in order to perform a simple optimization of the proposed detector structure.

1 Preparation and analysis of thin films

1.1 Ferroelectric film preparation

Most of the ferroelectrics have perovskite structure, with the molecular formula of ABO_3. The target is lead zirconate titanate ($PbZr_{0.52}Ti_{0.48}O_3$, PZT) produced by China New Materials (Beijing) Technology Co., Ltd. The target has a purity of 99.99%, a diameter of 75 mm, and a thickness of 3 mm. The substrate is $Pb/Ti/SiO_2/Si$. A MSP-300B automatic magnetron sputtering coating machine is used. The sputtering furnace is heated to 100 ℃, and the vacuum is 5×10^{-4} Pa. Working gas is high purity Ar. Experiments are preliminarily carried out to prepare PZT film samples with two different sputtering powers, and three different annealing conditions. Specific process parameters are listed in Tables 1 and 2, schematic diagram of PZT preparation structure is shown in Fig1.

Table 1 PZT film experimental sample process parameters

Experimental sample	Sputtering power/W	Working pressure /Pa	Sputtering time/h
1	100	1	1.50
2	200	1	0.75

Table 2　Annealing process parameters

Experimental sample	Annealing temperature/℃	Annealing time/min
1-A	650	3
1-B	700	3
1-C	750	3
2-A	650	3
2-B	700	3
2-C	750	3

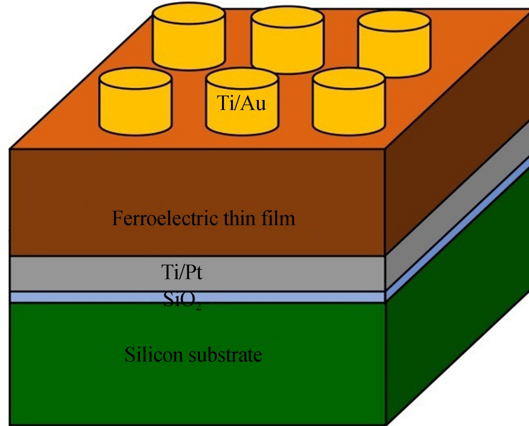

Fig.1　Schematic diagram of PZT preparation structure

1.2　Test analysis and discussion

1.2.1　*Surface topography*

As seen in Fig.2(a)～(c), there is no obvious crystal structure at a sputtering power of 100 W and an annealing temperature of 650 ℃. As the annealing temperature increases to 700 ℃, the grains grow significantly, but the surface of the film is somewhat convex, the film forms a structure other than perovskite[17]. When the annealing temperature rises to 750 ℃, the film has obvious cracks.

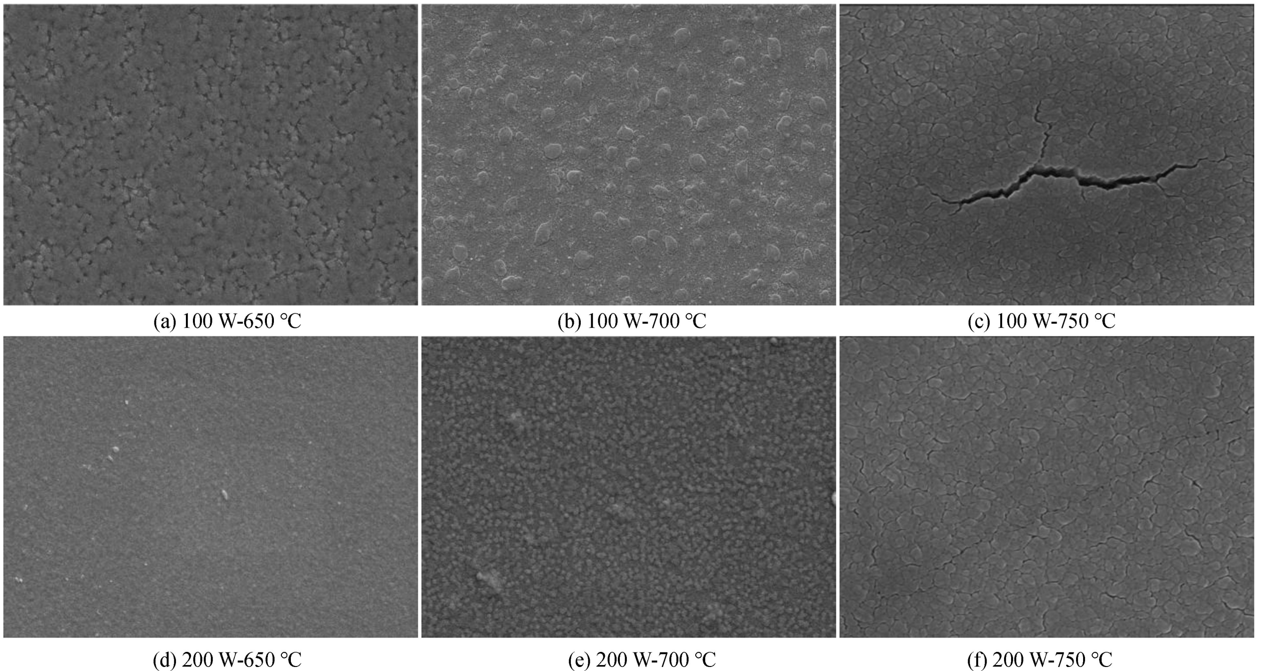

(a) 100 W-650 ℃　(b) 100 W-700 ℃　(c) 100 W-750 ℃

(d) 200 W-650 ℃　(e) 200 W-700 ℃　(f) 200 W-750 ℃

Fig.2　SEM morphologies

As it can be seen from Fig.2(d)～(f), at sputtering power of 200 W and annealing temperature of 650 ℃ the surface of the film is flat, and no significant grain structure appears. At this time, the film does not form a distinct crystal structure. When the annealing temperature is raised to 700 ℃, the film surface exhibits a distinct grain

structure, the grain size is uniform, and the spacing is relatively dense. When the annealing temperature finally rises to 750 ℃, the film shows fine cracks. This is because the growth of adjacent grains is hindered by stress, and the stress can not be released, resulting in the occurrence of cracks.

In summary, when the sputtering power is the same, the film annealed at 700 ℃ grows well. And at the same annealing temperature, the surface morphology of the film prepared by 200 W is better. Thus, according to the presented morphological analysis, the optimum growth conditions for the PZT film are a sputtering power of 200 W and an annealing temperature of 700 ℃.

1.2.2 *XRD phase analysis*

The crystalline properties of the PZT test samples fabricated under different conditions are evaluated by means of X-ray Diffraction (XRD) measurements. It is well-known that a preferred (111) growth orientation is advantageous for the performance of the ferroelectric film[18]. From Fig.3(a) we can see that the peaks relevant to the (110) and (111) orientations are the largest when the annealing temperature is 700 ℃. As the annealing temperature increases to 750 ℃, the peaks of both orientations clearly decrease. From Fig.3(b), we can also see that the (110) and (111) orientation peaks are also the largest when the sputtering power reaches 200 W and the annealing temperature is 700 ℃. In addition, when the annealing temperature is the same, the (111) growth orientation is larger for the sputtering power of 200 W, with respect to 100 W. From Fig.3(b) we can also see that, contrary to the 100 W sputtering rate, when the sputtering power reaches 200 W, for the 700 ℃ and 750 ℃ annealing temperatures the peak of the (111) orientation dominates over that of the (110) orientation, thereby indicating a preferred (111) growth.

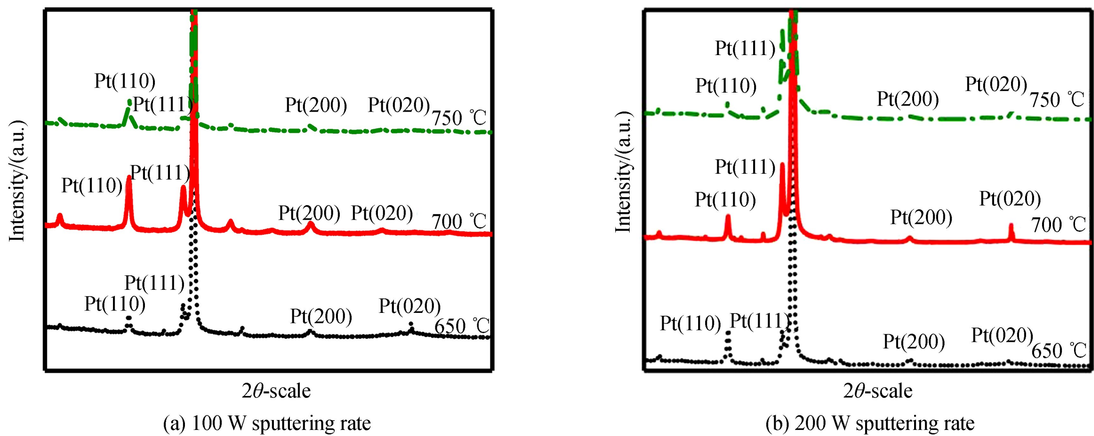

Fig.3 XRD analysis chart of different growth conditions

From the reported XRD analysis we can conclude that when the sputtering power is 200 W and the annealing temperature is 700 ℃, the lattice orientation of the film shows the best ferroelectric characteristics. Moreover, from the preparation process analysis, under larger sputtering power the crystal grains generated by the sputtering machine bombarding the target have a higher speed. This, in turn, results in a better adhesion of the crystal grains to the substrate, and the resulting PZT film is more dense.

1.2.3 *Hysteresis loop analysis*

The three key parameters from the hysteresis loops recorded by the ferroelectric test system are: the coercive field (E_c), the remnant polarization (P_r), and the saturation polarization (P_s)[19-20]. The greater the remnant polarization and the smaller the coercive field of the film, the better its ferroelectric performance. Fig.4(a) and Table 3, Fig.4(b) and Table4 show the hysteresis loops and parameters of the PZT ferroelectric thin films annealed at 650 ℃, 700 ℃ and 750 ℃ when the sputtering power is 100 W or 200 W, respectively.

We can see From Fig.4(a) and Table 3, the remnant polarization first increases, and then decreases as the annealing temperature increases. We can draw the same conclusion also from Fig.4(b) and Table 4. Indeed, as the temperature increases, the perovskite structure begins to grow, so the remnant polarization becomes larger. If the temperature continues to rise, and the Pb element is largely volatilized, resulting in an increase in film defects, and the remnant polarization is thus reduced. Therefore, a balance point can be defined as the best annealing temperature, which results to be 700 ℃.

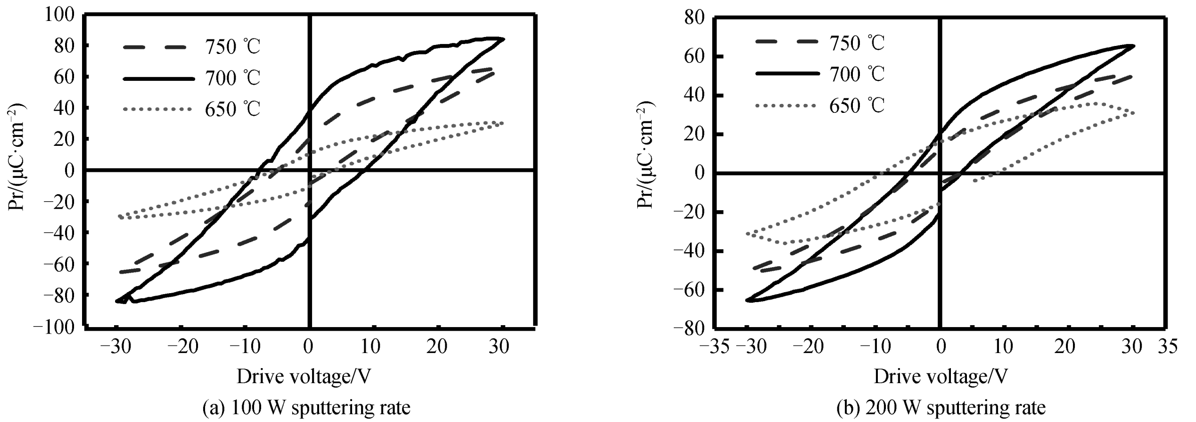

Fig.4　Analysis of hysteresis loops for different growth conditions

Table 3　Parameter results of Fig.4(a)

Annealing temperature/℃	Saturation polarization/(μC·cm^{-2})	Remnant polarization/(μC·cm^{-2})	Coercive field/(kV·cm^{-1})
650	30.6	9.3	37.0
700	65.3	20.4	31.5
750	50.8	12.4	33.7

Table 4　Parameter results of Fig.4(b)

Annealing temperature/℃	Saturation polarization/(μC·cm^{-2})	Remnant polarization/(μC·cm^{-2})	Coercive field/(kV·cm^{-1})
650	36.0	7.1	32.3
700	84.0	38.0	37.3
750	62.6	17.4	30.5

By comparing the remanent polarization and the coercive electric field of the PZT ferroelectric thin films annealed at 700 ℃ under the two evaluated sputtering power conditions, we can find that the residual polarization and the coercive electric field of the 200 W PZT thin film are greater and smaller, respectively, than those of the 100 W sample. In summary, on the whole, the 200 W sputtering power and 700 ℃ annealing temperature are the best growth conditions for the PZT ferroelectric thin films.

2　Sense grating HEMT device preparation and testing

2.1　Sense grating GaN HEMT preparation process

After the analysis of the basic HEMT device and of the optimization procedure for the fabricated PZT thin films, the new PZT/GaN-based HEMT detector structure is discussed in the following. A schematic diagram of the novel device design is shown in Fig.5.

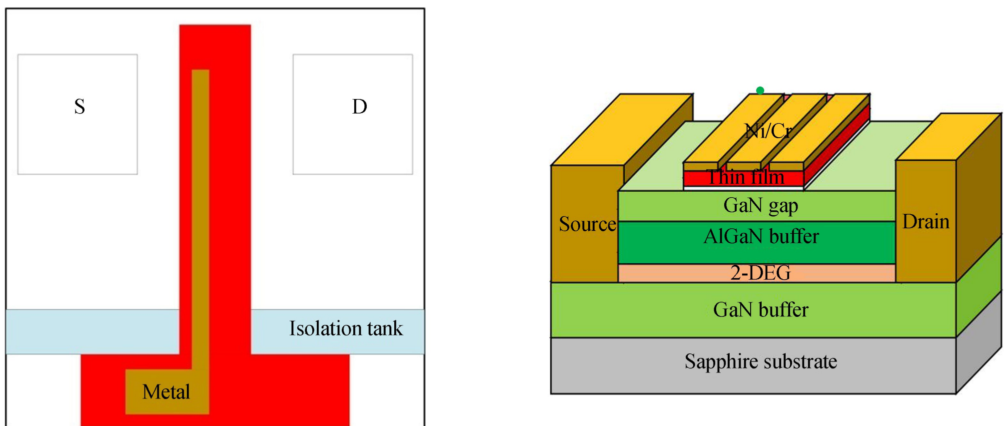

Fig.5　Schematic diagram of the PZT/GaN-based HEMT detector structure

The specific steps for the fabrication of the detector structure are schematically illustrated in Fig.6. They mainly include: cleaning epitaxial, inductively coupled plasma reactive ion etching (Inductively Coupled Plasma) for active area mesa definition, chemical vapor deposition of a SiO_2 (200 nm) isolation layer protecting the active region, source and drain electrode sputtering and annealing to form ohmic contacts, Ti/Pt gate electrode sputtering, and PZT grating film growth , sputtering of the upper electrode on the film.

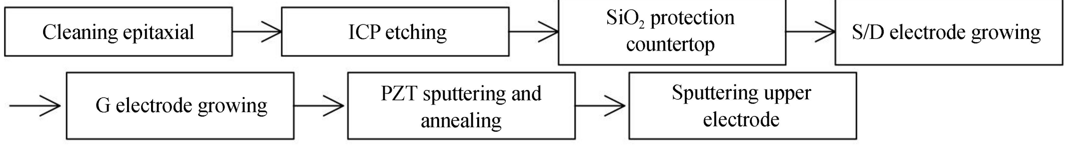

Fig.6 Illustration of the steps relevant to the fabrication of the grating electrode GaN-based HEMT device structure

2.2 Test analysis

The output characteristics of the HEMT detectors fabricated without and with the photosensitive gate are recorded under both dark condition and 365 nm wavelength UV illumination. In both cases test conditions are: V_{DS} ranging between 0 and 15 V, three sets of V_{GS} voltages are evaluated, namely −3 V, −2.5 V, and −2 V. A 5 W , 365 nm Light Emitting Diode (LED) is used as the UV light source, illuminating the device gate during tests.

The output characteristics plotted in Fig.7 indicate that the tested HEMTs are normally-on (depletion mode) devices. At a given gate voltage V_{GS} , as the source-drain voltage V_{DS} increases, the electron mobility in the channel starts to increase, the source-drain current I_{DS} increases as well, and the device enters the linear region. If the V_{DS} increases further, the electron mobility reaches the maximum, the I_{DS} reaches its maximum value, which is kept almost constant for higher drain-to-source voltages, and the device enters the saturation region. At a given source-drain voltage V_{DS}, as the gate voltage V_{GS} increases, the concentration of 2-DEG starts to increase, the source-drain current I_{DS} increases as well, so among the three evaluated gate voltages, the higher the gate voltage, the higher the device saturation current. During the test, we mainly focus on the changes of saturated source-drain current and saturated source-drain voltage before and after illumination.

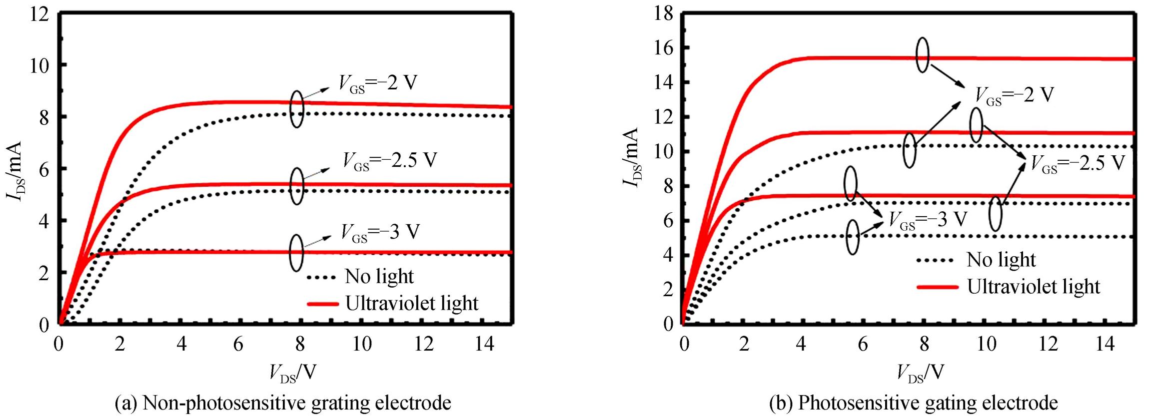

Fig.7 Dark and UV light output characteristic curves for the tested GaN-based HEMT devices

Fig.7(a) shows the source-drain output characteristics of a pristine HEMT detector, i.e., non-photosensitive grating electrode. Firstly, it can be observed that under UV irradiation, the device source-drain saturation current increases by 1.04 mA and 0.61 mA when V_{GS} is −2 V and −2.5 V, respectively. When V_{GS} is −3 V, the source-drain saturation current remains almost the same. Secondly, the UV light can saturate the source-drain current in advance. Indeed, when V_{GS} is −2 V, the saturation source-drain voltage V_{DS} decreasing by 1.85 V, at most. Thus, the non-photosensitive grating HEMT device does not respond significantly to ultraviolet light.

Fig.7(b) displays the output characteristics of the photosensitive gate HEMT device. It can be clearly seen that the novel detector structure exhibits a significant response to the UV light. Firstly, the source-

drain saturation current increases significantly by about 5.84 mA, 4.38 mA, and 2.34 mA when V_{GS} is −2 V, −2.5 V, and −3 V, respectively. Secondly, the saturation source-drain voltage V_{DS} drop by 3.55 V, at most.

According to the experimental results, it can be concluded that the non-photosensitive grating HEMT device exhibits some response to the UV light, which causes a drop in the device saturation source-drainvoltage, and increases the saturation source-drain current. This is because UV photons can excite electron-hole pairs in the AlGaN/GaN material, thereby increasing the 2-DEG density. However, the response to the UV irradiation of the photosensitive gate HEMT device is markedly larger. Indeed, a PZT ferroelectric thin film is specifically deposited on the metal gate of the GaN-based HEMT device as a light sensing layer. When the light impinges on the gate, the photosensitive PZT layer generates an additional electric field due to the photovoltaic effect, and finally acts on the 2-DEG thereby causing a change in the output current. On the whole, the proposed novel device structure clearly manages to better detect light[21].

3 Grid optimization

The source-drain output current is obviously affected by the gate voltage. The size of the gate length can regulate the gate voltage to change the output current. Reducing the gate length increases the device transconductance, which in turn increases the gate control capability of the device. However, a too short gate length affects the two-dimensional distribution of the potential under the gate, resulting in a short channel effect[22].

In this experiment, three different gate length devices are designed. Both the transfer and the output characteristics of the fabricated devices are measured at the same test conditions, under 365 nm wavelength UV light irradiation. The influence of the different gate lengths on the device response is analyzed too. This achieves the goal of optimizing device performance as well as improving device detection efficiency. The device structure parameters relevant to the different gate lengths are summarized in the Table 5. Fig.8 shows the physical maps of the three devices.

Table 5 Device structure parameters for the three different gate lengths

Sample label	Gate length(L_G/μm)	Gate source spacing(L_{GS}/μm)	Gatedrain spacing(L_{GD}/μm)
A	1	3	4
B	2	3	4
C	3	3	4

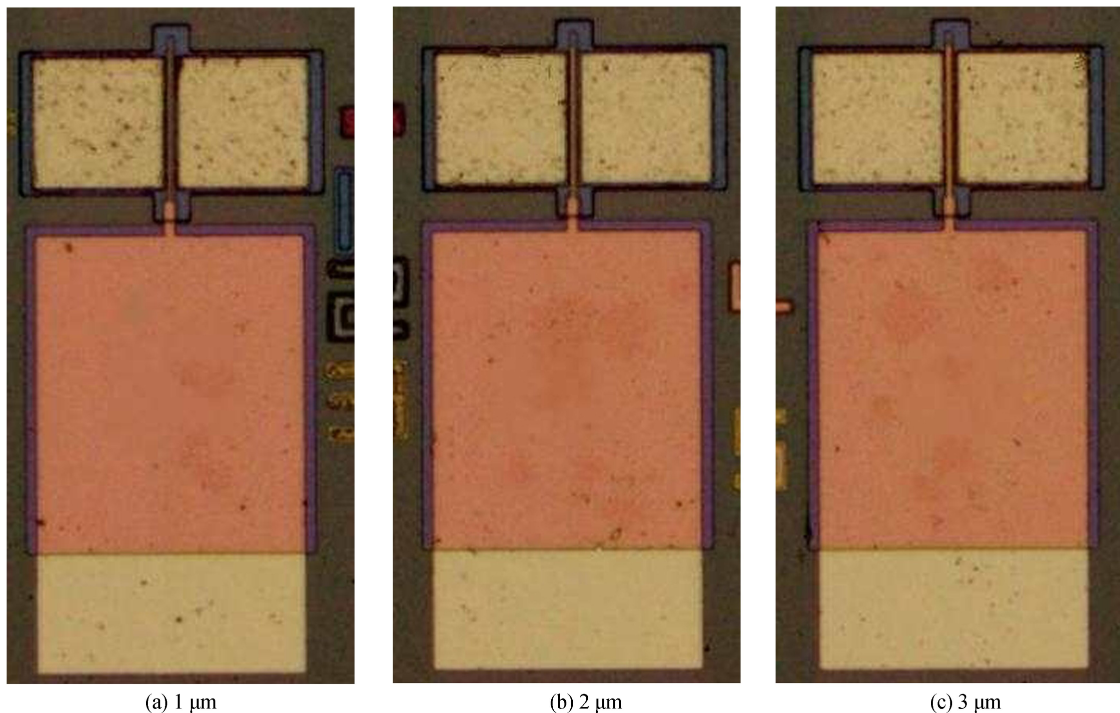
(a) 1 μm (b) 2 μm (c) 3 μm

Fig.8 Optical micrograph of the three kinds of different gate length devices

In the transfer characteristic curves, V_{GS} varies between −4 V and +2 V. The results are plotted in Fig.9(a). Clearly, as the gate length increases, the threshold voltage of the HEMT device becomes larger. In the output characteristics, V_{DS} ranges between 0 V and 15 V, and V_{GS} is set to −2 V. The results are displayed in Fig.9(b). The saturation currents of devices A, B, and C are 17 mA, 20 mA, and 23 mA, respectively. That is, the longer the gate, the smaller the device drain saturation current. Indeed, the longer the gate, the larger the width of the depletion layer below the gate, which causes the 2-DEG concentration to drop here, eventually causing the drain current to drop. Moreover, the increase in gate length leads to an increase in channel resistance, as well as to a longer carrier transport path, and to a knee voltage effect, which all lead to a decrease in the drain saturation current.

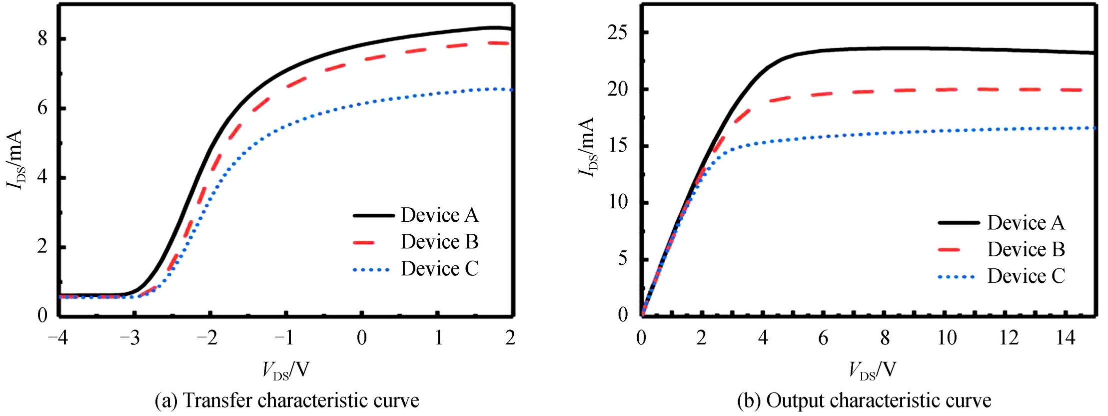

Fig.9 Characteristic curves of the three different gate length devices

The reported experimental results show that the photosensitive gate HEMT device specifically designed as a new type of photodetector not only exhibits a higher sensitivity to light, but also allows for improving the overall detection efficiency by changing its structural parameters. In the future, we can further improve the detection efficiency by improving other structural parameters of the device.

4 Conclusion

In this paper, a novel photosensitive gate GaN HEMT detector structure is proposed, based on the favorable photovoltaic effect in PZT ferroelectric thin films and on the characteristics of GaN HEMT devices. The output characteristics of the photosensitive gate HEMT device are measured under both dark conditions and illumination of ultraviolet light. It is found that the fabricated detector exhibits a significant photoresponse to ultraviolet light. Indeed, under illumination, the output current increases by 5.84 mA, and the saturation voltage drops by 3.55 V, at most. This is because when the light impinges on the photosensitive gate, an additional electric field is generated due to the photovoltaic effect in the PZT layer. This electric field acts on the 2-DEG, and the gate voltage control of the channel is achieved, thereby increasing the output current. Finally, three different gate length photosensitive gate HEMT devices are fabricated. It is found that the longer the gate, the smaller the source-drain output current of the device. This is due to the increase in gate length resulting in a decrease in 2-DEG concentration, and an increase in channel resistance. In summary, the proposed novel photosensitive gate GaN-based HEMT detector structure exhibits a high sensitivity to light. As a future work, the manufacturing process of both the ferroelectric thin film and the HEMT device will be further optimized to improve the detection performance.

References

[1] ZHANG Xi-sheng, YAN Chun-yu, WU Ti-hui, *et al*. Fabrication of $CsPbBrI_2$ quantum dots and its photodetector performance[J]. *Acta Photonica Sinica*, 2020, **49**(1): 123002.

[2] NANVER L, QI Lin, MOHAMMADI V, *et al*. Robust UV/VUV/EUV pureB photodiode detector technology with High CMOS compatibility[J]. *IEEE Journal of Selected Topics in Quantum Electronics*, 2014, **20**(6): 306-316.

[3] YANG Zhen-qian, DENG Yu-hao, ZHANG, Xiao-wei, *et al*. High-performance single-crystalline perovskite thin-film photodetector[J]. *Advanced Materials*, 2018, **30**(8): 1704333.

[4] AMBACHER O, FOUTZ B, SMART J, *et al*. Two dimensional electron gases induced by spontaneous and piezoelectric

polarization in undoped and doped AlGaN/GaN heterostructures[J]. *Journal of Applied Physics*, 2000, **87**(1): 334-344.

[5] CLAIRE G, HOCK M N, GEORGE CHU S N, *et al*. Intersubband absorption at λ1.55 μm in well- and modulation-doped GaN/AlGaN multiple quantum wells with superlattice barriers[J]. *Applied Physics Letters*, 2000, **77**(23): 3722-3724.

[6] ZHU J, ZHOU X, JING L, *et al*. Piezotronic effect modulated flexible AlGaN/GaN high-electron-mobility transistors [J]. *ACS Nano*, 2019, **13**(11): 13161-13168.

[7] CHEN C C, CHEN H I, LIU I P, *et al*. Enhancement of hydrogen sensing performance of a GaN-based Schottky diode with a hydrogen peroxide surface treatment[J]. *Sensors and Actuators B:Chemical*, 2015, **211**: 303-309.

[8] LI Jin-lun, CUI Shao-hui, ZHANG Jing, *et al*. Research of InP-based room temperature HEMT terahertz detector enhanced by butterfly antenna[J]. *Infrared and Laser Engineering*, 2019,**48**(9): 131-138.

[9] KHAN F, KHAN W, KIM S D. High-performance ultraviolet light detection using nano-scale-fin isolation AlGaN/GaN heterostructures with ZnO nanorods[J].*Nanomaterials*, 2019, **9**(3): 9030440.

[10] HU Zhi-jun, TIAN Ming-wen, NYSTEN B, *et al*. Regular arrays of highly ordered ferroelectric polymer nanostructures for non-volatile low-voltage memories[J]. *Nature Materials*, 2008, **8**(1): 62-67.

[11] BUTLER K T, FROST J M, WALSH A. Ferroelectric materials for solar energy conversion: photoferroics revisited [J]. *Energy&Environmental Science*, 2015, **8**(3): 838-848.

[12] CAI Tian-yi, JU Sheng. Photovoltaic effect in ferroelectrics[J]. *Acta Physica Sinica*, 2018, **67**(15): 157081.

[13] HAMATANI T, SHIRAHATA Y, OHISHI Y, *et al*. Arsenic and chlorine co-doping to CH3NH3PbI3 perovskite solar cells[J]. *Advances in Materials Physics and Chemistry*, 2017, **7**(1): 1-10.

[14] ZENKEVICH A V, MATVEYEV Yu, MAKSIMOVA K, *et al*. Giant bulk photovoltaic effect in thin ferroelectric $BaTiO_3$ films[J]. *Physical Review B*, 2014, **90**(16): 161409(R).

[15] LI Xiong, YI Chen-yi, LUO Jing-shan, *et al*. Improved performance and stability of perovskite solar cells by crystal crosslinking with alkylphosphonic acid ω-ammonium chlorides[J]. *Nature Chemistry*, 2015,**7**(9): 703-711.

[16] LEE Chun-hsun, LIN Wei-ren, LEE Yu-hsuan, *et al*. Characterizations of enhancement-mode double heterostructure GaN HEMTs with gate field plates[J]. *IEEE Transactions on Electron Devices*, 2018, **65**(2): 488-492.

[17] TAKAYUKI T, MASAKI M, TAKAYUKI K, *et al*. Fabrication of L10-FeNi phase by sputtering with rapid thermal annealing[J]. *Journal of Alloys & Compounds*, 2018, **750**: 164-170.

[18] ZHENG Fen-gang, CHEN Jian-ping, LI Xin-wan. Improved dielectric and ferroelectric characteristics of highly (111)-oriented Pb(Zr0.52Ti0.48)O3 films produced by Sol-Gel method[J]. *Acta Physica Sinica*, 2006, **55** (6): 3067-3072.

[19] SUN Ke-xue, ZHANG Shu-yi, SHUI Xiu-ji, *et al*. Experimental and numerical study on transverse piezoelectricity of x BiInO 3-(1-x) $PbTiO_3$ films by multilayer cantilevers[J]. *Japanese Journal of Applied Physics*, 2018, **57**(2): 025801.

[20] SUN En-wei, ZHANG Rui, ZHAO Xin, *et al*.Electro-optic properties of relaxor ferroelectric $0.93Pb(Zn_{1/3}Nb_{2/3})O_3$-$0.07PbTiO_3$ single crystal[J].*Acta Photonica Sinica*.2009,**38**(6): 1442-1445.

[21] QIAO Hong, YUAN Jian, XU Zai-quan, *et al*. Broadband photodetectors based on graphene-Bi_2Te_3 heterostructure[J]. *ACS Nano*, 2015,**9**(2): 1886-1894.

[22] PARK P S, RAJAN S. Simulation of short-channel effects in N-and Ga-Polar AlGaN/GaN HEMTs[J]. *IEEE Transactions on Electron Devices*, 2011, **58**(3): 704-708.